Pyrite in contact with supercritical water: The desolation of steam

András Stirling,*[a] Tamás Rozgonyi,[b] Matthias Krack,[c] Marco Bernasconi[d]

Received Xth XXXXXXXXXX 20XX, Accepted Xth XXXXXXXXX 20XX
First published on the web Xth XXXXXXXXXX 200X
DOI: 10.1039/b000000x

Supercritical water - pyrite interface has been studied by ab initio molecular dynamics simulation. Extreme conditions are relevant in the *iron-sulfur world, ISW* theory where prebiotic chemical reactions are postulated to occur at the mineral-water interface. We have investigated the properties of this interface under such conditions. We have come to the conclusion that hot-pressurized water on pyrite leads to an interface where a dry pyrite surface is in contact with the nearby SC water without significant chemical interactions. This picture is markedly different from that at ambient conditions where the surface is fully covered with adsorbed water molecules which is of relevance for the surface reactions of the ISW hypothesis.

1 Introduction

Pyrite is a semiconducting mineral playing an important role in various geochemical and environmental processes[1]. In the last decades FeS_2 has also been given intense attention as a promising photovoltaic device[2]. Pyrite also appears in the Iron-Sulfur-World (ISW) scenario of Wächtershäuser where iron-sulfide minerals act as catalysts and reactants in reactions leading to the formation of prebiotic molecules in hot-pressurized water[3,4]. The extreme (most often supercritical (SC)) conditions alter remarkably the rate of the reactions occurring in water[5]. This is due to the properties of SC water, such as low dielectric constant, increased acidic and basic properties, fewer and weaker H-bonds and higher compressibility[6]. In the context of ISW hypothesis SC conditions present in deep sea hydrothermal vents are assumed to promote the reactions taking place on iron-sulfide mineral surfaces. A number of experiments have provided convincing support, and the catalytic role of iron-sulfide minerals, pyrite in particular, has been demonstrated[7–12]. Several quantum chemical metadynamics calculations have also been performed to study the steps leading to the peptide bond formation on FeS_2 surface where the roles of surface defects and the hot-pressurized water in the mechanism have also been discussed: exposed iron surface sites have increased reactivities; sulfur vacancies can efficiently bind potential reactants (e.g. amino acids) with higher retention times; and higher temperature can efficiently decrease activation free energy barriers[13–17].

A central role has been attributed to pyrite in the ISW prebiotic chemistry as adsorbent, reactant and catalyst[3,10–12]. It has been already shown that in water at ambient conditions the most stable pyrite (100) surface is fully covered by adsorbed water molecules binding on surface iron atoms[18–20]. This exposes the surface sulfur atoms to potential nucleophilic attacks because on wet FeS_2 surfaces the LUMOs (edge of the conduction band) are localized on the surface S atoms. In contrast, on dry pyrite surfaces the lowest empty atomic orbitals are on the surface Fe(II) sites hinting different reactivities[19]. This sensitivity of the surface electronic structure points to a remarkable coverage-dependent reactivity which may be tuned by varying the conditions. Therefore a detailed insight into the pyrite-water interface at SC conditions is necessary to address the mechanisms of the reactions occurring at the interface of pyrite and SC water. To this end, we have performed ab initio molecular dynamics (MD) simulations of hot-pressurized water in contact with FeS_2 employing perfect and defective pyrite surfaces and characterized the interfacial water and the dynamic aspects of the SC water–pyrite interaction.

2 Models and Methods

We performed Born-Oppenheimer molecular dynamics simulations by using the CP2K package[21]. The electronic structure has been described by density functional theory (DFT) using the Perdew-Burke-Ernzerhof (PBE) functional[22]. The valence orbitals have been expanded using short range, molecularly optimized (MOLOPT-SR) double-ζ basis sets[23]. For the S, O and H atoms the basis was augmented by a set of polarization functions (DZVP). The electronic charge density has been expanded in an auxiliary basis set of plane waves with

[a]*Institute of Organic Chemistry, Research Centre for Natural Sciences of the Hungarian Academy of Sciences, Budapest, Hungary, E-mail: stirling.andras@ttk.mta.hu*
[b]*Institute of Materials and Environmental Chemistry, Research Centre for Natural Sciences of the Hungarian Academy of Sciences, Budapest, Hungary*
[c]*Laboratory for Reactor Physics and Systems Behaviour, Paul Scherrer Institute, CH-5232 Villigen PSI, Switzerland*
[d]*Department of Materials Science, University of Milano-Bicocca, I-20125 Milano, Italy*

a kinetic energy cutoff of 400 Ry. Only the Γ-point has been considered for the *k*-point sampling. The interaction between the valence electrons and the ionic cores have been described with GTH pseudopotentials optimized to the selected basis set and functional[24]. The present setup has resulted in nonmagnetic ground state and throughout the calculations we have kept this state. Our methodology gives an optimal cell constant of 5.417 Å with a 96-atom supercell which compares very nicely with experiment (e.g. 5.416 Å[25],5.428 Å[26]). The predicted band-gap is 0.4 eV (generally accepted experimental value[27] is 0.95 eV). This underestimation is typical for functionals applying only standard semilocal approximations[28] but this feature does not effect the main conclusions here as evidenced by earlier studies[16,19,29,30].

The pyrite-water interface has been modeled in a slab geometry with 12 pyrite layers (Fig 1). Each layer contains 8 iron or sulfur atoms, ie. a 2×2 surface supercell. The bottom iron layer has been terminated by water molecules attached to iron atoms to provide bulk-like conditions[19]. The periodically repeated slabs are separated by a $\sim$ 14 Å water layer. The size of the unit cell is $10.8348 \times 10.8348 \times 26.8348$ Å^3. Two surface models have been considered: a surface representing the perfect (100) plane and another featuring a surface S-vacancy site, ie. missing one of the top S atoms. On this surface there are two 4-coordinated (defective) surface iron sites. A typical SC state has been selected as 800 K and 0.1 GPa which is equivalent with a density of 0.5 g/cm^3 according to the water equation of state[31]. The space between the pyrite slabs has been filled with 28 water molecules which corresponds to this density. Note however, that the available volume is not well-defined therefore the density and the corresponding pressure is only approximately determined by the number of the H_2O molecules.

A constraint has been applied to the bottom 3 FeS_2 layers and the O atoms of the terminating water molecules and they have been kept fixed while all the other degrees of freedom were allowed to freely move. The NVT conditions have been enforced employing the velocity rescaling thermostat of Bussi et al.[32] with a coupling time constant of 1 ps. The time step for integrating the Verlet equations was 0.4 fs. After an initial structural optimization and a gradual heating to 800 K, a $\sim$ 20 ps equilibration has been performed. Then the trajectories have been followed for another period of $\sim$ 20 ps.

3 Results

3.1 Characterization of the water

The surface properties of pyrite have been studied thoroughly both experimentally[1,33] and theoretically[19,30,34,35]. The most important conclusions in relation to the FeS_2-water interface are the following: i) surface iron atoms are the primary sites for water adsorption[19,30,36,37]; ii) surface iron charge states are weakly affected by water adsorption as evidenced by experimental and theoretical core level shift analysis[1,30,38]; iii) in contrast, their reactivity is strongly affected by their coordination: four coordinated (defective) iron atoms can bind more tightly adsorbed molecules as compared to a five coordinated surface iron atom[15,30]; iv) molecular adsorption is preferred to dissociative adsorption on both the normal and defective surfaces[15,19,30].

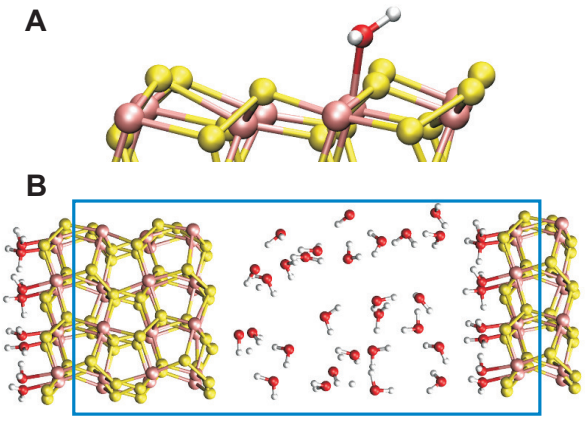

Fig. 1 Simulation model. A: defective surface with a temporarily adsorbed water molecule on one of the defective (4-coordinated) Fe(II) sites. B: full periodic interface model. The unit cell is indicated by a blue frame.

Before analyzing the water-pyrite interface it is useful to look into the properties of the simulated water because this can provide a measure how efficient the methodology is. To this end we have calculated quantities characteristic of bulk water. Note that the limited size and the heterogeneous nature of the system complicates the application of concepts which are valid for homogeneous systems. Fig. 2 shows the mean square displacement (MSD) of the water molecules in both systems. We have calculated MSDs in 3D and also the in-plane (2D) MSDs to see the effect of confinements. All curves show linear behavior which allows the estimation of diffusivity by linear fitting and applying eq. 1:

$$2dD = \frac{\partial \left\langle r^2(t) \right\rangle}{\partial t} \qquad (1)$$

where D is the self diffusion coefficient, d is the dimensionality of the system, $r(t)$ is the distance travelled by a water molecule during time t. The DFT methodology applied here has been shown to reproduce nicely the experimental diffusion coefficients at different SC conditions.[39] The estimated 3D diffusion coefficients are 5.4 and 5.3 $\cdot 10^{-8} m^2/s$ for the normal and defect surfaces, respectively. Larger diffusivities have been obtained by taking into account only the

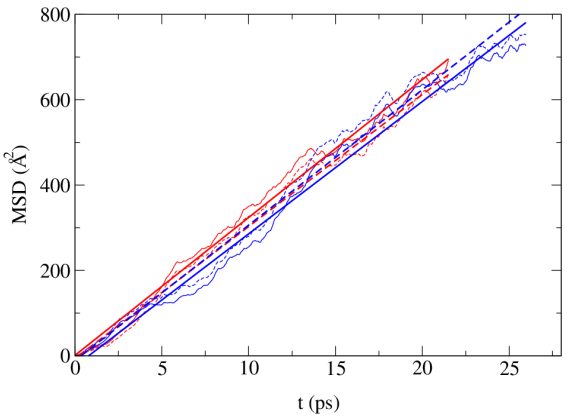

Fig. 2 Mean square displacements as a function of time. Red: on normal surface; blue: on defective surface. Solid line: total displacement; dashed line: displacement parallel to the xy directions. Fitted straight lines are also shown.

movements parallel to the surface plane: $7.7 \cdot 10^{-8} m^2/s$ in both cases. Clearly, this latter value is more realistic as it is less affected by the limited thickness of the water. In fact it shows fortuitously excellent agreement with the experimental $7.74 \cdot 10^{-8} m^2/s$ value[40]. The simulations clearly indicate that the presence of defect has no measurable effect on the interfacial diffusion. Note however, that during the simulations temporal adsorption of limited number of water molecules occurs (*vide infra*), therefore the diffusivities are slightly underestimated[41].

The hydrogen bond network plays an important role in the properties of water, even at extreme conditions. We have therefore calculated the average number of H-bonds per molecules. The H-bond estimation is based on the definition described in Ref.[42]. For the presence of a H-bond between two water molecules we calculated the h_{ij} function as a product of two terms:

$$h_{ij} = \frac{1-\left(\frac{r_{ij}-C}{r_O}\right)^{10}}{1-\left(\frac{r_{ij}-C}{r_O}\right)^{20}} \cdot \sum_k^H \frac{1-\left(\frac{r_{ik}+r_{jk}-r_{ij}}{r_H}\right)^8}{1-\left(\frac{r_{ik}+r_{jk}-r_{ij}}{r_H}\right)^{12}}$$

where the $C = 2.7$Å, $r_O = 0.5$ Å and $r_H = 0.6$ Å. The first term is nonvanishing if the distance r_{ij} between the O_i and O_j atoms of the two water molecules is smaller than 3.5 Å and takes the maximal value 1 when it is around 2.7 Å. The second term is 1 if $r_{O_iH_k} + r_{O_jH_k} - r_{O_iO_j}$ is 0 and gradually vanishes as this sum exceeds 0.6. We find that in average a water molecule forms 0.8 hydrogen bond and the distribution of the H-bond number is strictly localized around values 0 and 1. We note that applying other H-bonding criteria yields very similar results.[43] Our results are in line with experiment[44] and simulations[44,45] which also demonstrated significant loss of the H-bond numbers at various SC conditions as compared to ambient water.

3.2 Characterization of water adsorption

During the initial setup of the models 8 water molecules have been arranged on the FeS_2 surface in their optimal adsorbed positions at the iron sites at both sides of the slabs (for adsorption configurations see the terminated pyrite surface side in Fig. 1B)[15,19,30]. However, during the heating and in the subsequent runs the non-constrained H_2O molecules preferred to stay in the bulk water. This indicates that in hot-pressurized water the mineral surface is hardly covered by water. Partial desorption tendency at 500 K at water density of 0.85 g/cm^3 has been reported earlier by Marx et al.[14], but they have not explored this direction further. The distributions of the water molecules in the interfaces are plotted in Fig. 3. The curves show that the average densities are close to the

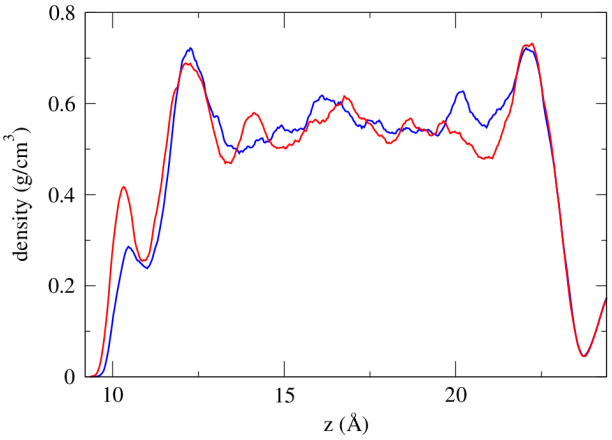

Fig. 3 Density profiles along the crystallographic *c*-axis, averaged out in xy directions. Blue: normal surface; red: defective surface. The origin of the axis is at the bottom of the pyrite slab. The iron atoms in the top pyrite layer can be found between 8.0-8.2 Å along the *c*-axis. The uphill of the density profiles around 25 Å is due to the fixed bottom water layer from the next periodic image. Bin size: 0.034 Å.

expected *ca.* 0.5 g/cm^3. However, at the edges of the bulk-like water the density peaks indicate a wall effect. It is also seen that a smaller peak appears on both profiles close to the pyrite surfaces. It is larger for the defective surface. These are the contributions of the temporarily adsorbed water molecules. Clearly, the higher peak indicates more frequent adsorption on the defective surface.

In order to estimate the coverage from the temporal adsorptions, we have defined the adsorption state with the distance between a surface iron and a water molecule as $d_{Fe-O} \leq 2.9$ Å. This criterion is based on the density distribution curves: it is the position of the first minimum after the first peak on the

density profiles with respect to the topmost iron level of the pyrite slab. With this criterion in hand we computed the probability of the iron sites to be occupied by a water molecule. In this way we have obtained 0.11 and 0.16 fraction of monolayer for the normal and defective FeS_2 surfaces, respectively. The values indicate that under SC conditions the pyrite is hardly covered with water. At variance with pyrite at ambient water[18–20], here the surface atoms are fully exposed in most of the time.

Further dynamical insight into the pyrite-water interface can be obtained by considering the kinetics of the desorption process. This can be done by calculating the population autocorrelation function.

$$C(t) = \frac{\langle h(0) \cdot h(t) \rangle}{\langle h(0) \rangle} \tag{2}$$

where $h(t) = 1$ if a given Fe site is continuously bonded to a water molecule from time 0 to t and otherwise $h(t) = 0$. This function is in fact the conditional probability density of finding a site continuously populated till time t if it was populated at time 0. A site is considered populated if $d_{Fe-O} \leq 2.9$ Å. The calculated autocorrelation functions are plotted in Fig. 4.

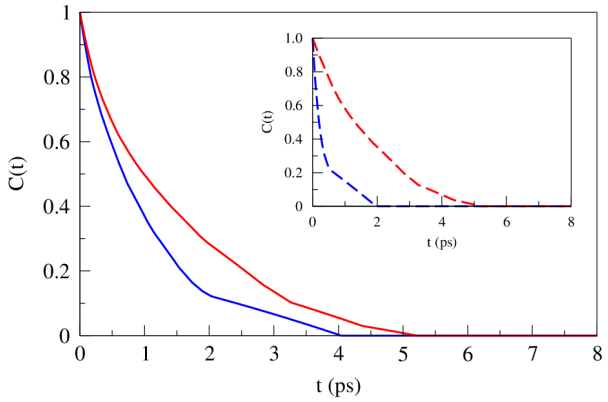

Fig. 4 Continuous population autocorrelation functions of water binding on iron sites of FeS_2 (100) surface. Blue: normal surface; red: defective surface. Inset: The same functions calculated for different sites on the defective surface. Blue: 5-coordinated surface iron atoms; red: 4-coordinated (defective) surface iron atoms.

An exponential decay of the correlation function indicates pure first-order kinetics. As Fig. 4 shows, this is not the case here, the curves show non-exponential behavior. However, simple exponential fitting can yield approximate characteristic mean lifetimes: 1.0 ± 0.3 and 1.5 ± 0.5 ps for the normal and defective surfaces, respectively[46]. In agreement with its higher reactivity defect surface can bind H_2O molecules more strongly. We note that eliminating the fast water in-out dynamics at the boundary defined by the bonding criterion yields only 0.1 ps variation in the lifetimes. The above population function effectively filters out situations where a given water molecule desorbs only for a very short period and then rebinds. To include these dynamically fast events we also calculated the population autocorrelation function of the *intermittent* population function $h_{int}(t)$. $h_{int}(t) = 1$ if a given Fe site is populated at time t, otherwise 0. From the decay of the corresponding autocorrelation functions we obtain the same lifetime for the normal surface but a somewhat longer, 2.3 ps lifetime value for the defective surface.

We can distinguish between the reactivities of the normal and defective iron sites by specifically calculating their occupation correlation functions. These are plotted in the inset of Fig. 4. Assuming first-order desorption kinetics we can obtain 0.4 ± 0.1 and 1.8 ± 0.5 ps for the normal (5-coordinated) and defective (4-coordinated) sites, respectively. It is seen that water mostly adsorbs on the defective sites, and the lifetime of the adsorbed states is significantly longer than that of an adsorption on a normal, 5-coordinated iron ion. We also see that on the defective surface, water adsorption on a normal iron site situated within the close vicinity of a defect has shorter average lifetime (0.4 ± 0.1 ps) than what obtained for irons on the normal surface (1.0 ± 0.3 ps). Earlier calculations on pyrite surface have shown that simultaneous water adsorption on neighbor iron sites changes the iron-water bond strength[19,47]. However simultaneous adsorption on a normal and a defective site is very rare during the simulations, therefore we attribute this discrepancy to the limited statistics[41].

The kinetic parameters of the desorption can be also predicted by explicitly assuming first-order (exponential) decay. Eq. 3 is a simple Arrhenius equation associated to the desorption in vacuum where the barrier to surmount is the binding energy of a water molecule on pyrite surface which amounts to 13 kcal/mol on a 5-coordinated iron(II) site[48].

$$k = \nu \exp\left(-\frac{E_b}{RT}\right) \tag{3}$$

where E_b is the calculated binding energy, and ν is the stretching frequency of the Fe-OH_2 unit (417 cm^{-1}) for approximating the desorption attempt frequency[19]. At 800 K we obtain $3.5 \cdot 10^9$ 1/s for the rate constant which translates to a 0.3 ns mean lifetime. This value is roughly two orders of magnitude larger than those obtained from the simulations and indicates an accelerated water desorption in the presence of SC water as compared to desorption in vacuum. The much faster desorption of the adsorbed water can be attributed to the energy gain by interacting with the SC water layer. Consistently with a roughly five times longer lifetime obtained for water adsorption on the defective sites compared to adsorption on normal iron sites, the calculated 16 kcal/mol adsorption energy on 4-

coordinated iron[15,30] gives a mean lifetime of 1.9 ns from the Arrhenius estimation. Although eq. 3 is based on simplifying assumptions, the huge discrepancies between the calculated mean lifetimes along with the observed non-exponential decays indicate that beside the elevated temperature, the presence of SC water plays a significant role in the very rapid loss of water from the pyrite surface.

4 Concluding remarks

Our results show that at SC conditions the water/pyrite interaction results in an almost completely dry surface even when defective (ie. more reactive) sites are present. The present findings have important implications to the reactivity of pyrite. The SC conditions effectively eliminate the water adsorption layer from the surface and expose the topmost atoms and defective sites. Therefore both the iron and sulfur sites are available and a wide range of reactions is facilitated without prior water desorption. They may be further enhanced by the unique properties of SC water exploited beneficially in chemical reactions.[5,6] In short, SC conditions result in dramatic changes at the pyrite-water interfaces which have to be taken into account in interpreting the kinetics and mechanism of reactions taking place at the interface. Exploration of this reactivity in redox processes is now underway and will be reported in due course.

5 Acknowledgment

Support of OTKA Grant K101115 is acknowledged. This work was supported by a grant from the Swiss National Supercomputing Centre (CSCS) under project ID s427.

References

1 Murphy, R.; Strongin, D. R. *Surf. Sci. Rep* 2009, **64**, 1-45.
2 C. Wadia, A. P. Alivisatos, D. M. Kammen, *Environ. Sci. Technol.*, 2009, **43** 2072-2077.
3 G. Wächtershäuser, *Microbiol. Rev.*, 1988, **52**, 452-484. G. Wächtershäuser, Prog. Biophys. *Mol. Biol.*, 1992, **58**, 85-201.; E. Drobner, H. Huber, G. Wächtershäuser, D. Rose, K. O. Stetter, *Nature*, 1990, **346**, 742-744.; E. Blöchl, M. Keller, G. Wächtershäuser, K.O. Stetter, *Proc. Natl. Acad. Sci. USA*, 1992, **89**, 8117 (1992). K.Ruiz-Mirazo, C. Briones, A. de la Escosura, *Chem. Rev.*, 2014, **114**, 285-366.
4 L.E. Orgel, *Trends. Biochem. Sci.*, 1998, **23**, 491-495.
5 A. Baiker, *Chem. Rev.*, 1999, **99**, 453-473.; N. Akiya, P. E. Savage, *Chem. Rev.*, 2002, **102**, 2725-2750.
6 H Weingärtner, E. U. Franck, *Angew. Chem. Int. Ed.*, 2005, **44**, 2672-2692.
7 C. Huber, G. Wächtershäuser, *Science*, 1997, **276**, 245-247.
8 C. Huber, G. Wächtershäuser, *Science*, 1998, **281**, 670-672.
9 C. Huber, G. Wächtershäuser, *Science*, 2006, **314**, 630-632.
10 J. A. Brandes, N. Z. Boctor, G. D. Cody, B. A. Cooper, R. M. Hazen, H. S. Yoder, Jr., *Nature*, 1998, **395**, 365-367.
11 G. D. Cody, N. Z. Boctor, T. R. Filley, R. M. Hazen, J. H. Scott, A. Sharma, H. S. Yoder Jr. *Science*, 2000, **289**, 1337-1340.
12 G. D. Cody, N. Z. Boctor, j. A. Brandes, T. R. Filley, R. M. Hazen, H. S. Yoder Jr. *Geochim. Cosmochim. Acta*, 2004, **68**, 2185-2196.
13 C. Boehme, D. Marx, *J. Am. Chem. Soc.*, 2003, **125**, 13362-13363.
14 R. Pollet, C. Boehme, D. Marx, *Orig. Life Evol. Bios.*, 2006, **36**, 363-379.
15 N. N. Nair, E. Schreiner, D. Marx, *J. Am. Chem. Soc.*, 2006, **128**, 13815-13826.
16 E. Schreiner, N. N. Nair, D. Marx, *J. Am. Chem. Soc.*, 2008, **130**, 2768-2770.
17 E. Schreiner, N.N. Nair, C. Wittekindt, D. Marx, *J. Am. Chem. Soc.*, 2011, **133**, 8216-8226.
18 S. Meis, U. Magdans, X. Torrelles, *Acta Cryst.*, 2011, **A67**, C338-C339.
19 A. Stirling, M. Bernasconi, M. Parrinello, *J. Chem. Phys.*, 2003, **118**, 8917-8926.
20 M. R. Philpott, I. Y. Goliney, T. T. Lin, *J. Chem. Phys.*, 2004, **120**, 1943-1950.
21 The CP2K Developers Group. Available at: www.cp2k.org; J. VandeVondele, M. Krack, F. Mohamed, M. Parrinello, T. Chassaing, J. Hutter, *Comput. Phys. Commun.*, 2005, **167**, 103-128.
22 J. P. Perdew, K. Burke, M. Ernzerhof, *Phys. Rev. Lett.*, 1996, **77**, 3865-3868.
23 J. VandeVondele, J. Hutter, *J. Chem. Phys.*, 2007, **107**, 114105.
24 S. Goedecker, M. Teter, J. Hutter, *Phys. Rev. B*, 1996, **54**, 1703-1710.; M. Krack, *Theor. Chim. Acta*, 2005, **114**, 145-152.
25 E. D. Stevens, M. L. DeLucia, P. Coppens, *Inorg. Chem.*, 1980, **19**, 813-820.
26 S.L. Finklea, L. Cathey and L. Amma, *Acta Crystallogr. A*, 1976, **32**, 529-537.
27 A. Ennaoui, S. Fiechter, C. Pettenkofer, N. Alonso-Vante,K. Büker, M. Bronold, C. Höpfner, H. Tributsch, H. *Sol. Energy Mater. Sol. Cells*, 1993, **29**, 289-370.
28 J. P. Perdew, R. G. Parr, M. Levy, J. L. Balduz, *Phys. Rev. Lett.*, 1982, **49**, 1691-1694.
29 A. Stirling, M. Bernasconi, M. Parrinello, *J. Chem. Phys.*, 2003, **119**, 4934-4939.
30 A. Stirling, M. Bernasconi, M. Parrinello, *Phys. Rev. B*, 2003, **75**, 165406.
31 A. Saul, W. Wagner, *J. Phys. Chem. Ref. Data*, 1989, **18**, 1537-1564.
32 G. Bussi, D. Donadio, M. Parrinello, *J. Chem. Phys.*, 2007, **126**, 014101.
33 a) K. M. Rosso, D. J. Vaughan, *Revs. Miner. Geochem.*, 2006, **61**, 505-556.; b) K. M. Rosso, D. J. Vaughan, *Revs. Miner. Geochem.* 2006, **61**, 557-607.
34 A. Hung, J. Muscat, I. Yarowsky, S. P. Russo, *Surf. Sci.*, 2002, **513**, 511-524.
35 G. U. von Oertzen, W. M. Skinner, H. W. Nesbitt, *Phys. Rev. B*, 2005, **72**, 235427.
36 F. Zipoli, R. Car, M. H. Cohen, A. Selloni, *J. Am. Chem. Soc.*, 2010, **132**, 8593-8601.
37 C. Pettenkofer, W. Jaegermann, M. Bronold, *Ber. Bunsenges. Phys. Chem.*,1991, **95** 560-565.
38 T. Kendelewicz, C. S. Doyle, B. C. Bostick, and G. E. Brown, Jr., *Surf. Sci.*, 2004, **558**, 80-88.
39 M. Boero, K. Terakura, T. Ikeshoji, C. C. Liew, M. Parrinello, *J. Chem. Phys.*, 2001, **115**, 2219-2227.
40 The experimental value was derived using the fitted polynomial expression (at $T = 800\ K$ and $\rho = 0.5\ \mathrm{g/cm^3}$) which has been published in: K. Yoshida, N. Matubayasi, Y. Uosaki, M. Nakahara, *J. Chem. Eng. Data*, 2010, **55**, 2815-2823.
41 As we show in the followings, the coverage is so low for both the normal and the defective surfaces that on average 0.9 and 1.3 water molecule is

fixed by adsorption, respectively. The difference of the errors caused by adsorption is small (there are 28 SC water molecules), therefore the diffusion coefficients are very similar for the two interfaces.

42 D. Donadio, P. Raiteri, M. Parrinello, *J. Phys. Chem B*, 2005, **109**, 5421-5424.

43 For example, we have tested the criterion used by Pártay et al for supercritical water: L. B. Pártay, P. Jedlovszky, I. Brovchenko, A. Oleinikova, *J. Phys. Chem B*, 2007, **111**, 7603-7609. In this case we have obtained for the average H-bond number 0.9. Note that Parrinello et al have assessed that this type of definition for H-bonding is qualitatively equivalent to more standard ones involving the angle between the OO and OH bonds or the interaction energy between the molecules: P. Raiteri, A. Laio, M. Parrinello, *Phys. Rev. Lett.* 2004, **93**, 087801.

44 Q. Sun, Q. Wang, *J. Phys. Chem. B*, 2014, **118**, 11253-11258.

45 R. Jonchiere, A. P. Seitsonen, G. Ferlat, A. M. Saitta, R. Vuilleumier, *J. Chem. Phys.*, 2011, **135**, 154503.

46 Standard errors have been estimated by block-averaging analysis dividing the trajectories into 4 pieces.

47 F. Zipoli, R. Car, M. H. Cohen, A. Selloni, *J. Chem. Theory Comput.*, 2010, **6**, 3490-3502.

48 The calculations employed similar setup (see Ref. [19]). Even stronger Fe-water bond was predicted by Zipoli et al (15.7 kcal/mol, Ref. [36]).

TOC entry:

Supercritical water and pyrite interface has been studied by DFT calculations. A surprisingly dry surface has been found which points to a new reactivity under extreme conditions which has relevance in the *Iron-Sulfur World* prebiotic chemistry of the early Earth .